Vanadium-bearing titaniferous-magnetite mineralization from the Simdega area, Chhotanagpur Gneissic Complex, Eastern India

Vanidiferous titano-magnetite occurrences are common in gabbro–norite–anorthosite associations all over the world[1]. Such type of ores are also reported from different parts of the Indian shield, viz. (i) Dublabera–Katwarpahar[2,3], Kumardhubi, Betjharan, Amdabera[4,5], Saltora[6] and Nausahi[7,8] areas of the Singhbhum craton, and (ii) the Nuggihali schist belt[9,10], Dharwar craton. In all these occurrences, the vanadiferous titano-magnetite ore bodies occur in the form of layers, lenses, pockets, stringers and veins. In this communication, we report the vanadium-bearing titaniferous magnetite disseminations from a gabbroic dyke near Saghjohr (22°36′15.9″N, 84°14′6.1″E), Simdega area, which is located about 60 km north of Manoharpur–Chiria iron ore deposit within the Chhotanagpur Gneissic Complex (CGC).

The Singhbhum craton, the Singhbhum mobile belt, CGC, and the Shillong plateau – together constitute the Eastern Indian shield (Figure 1 *a*). The CGC has experienced poly-phase deformation, metamorphism and magmatism[11,12]. Magmatism in CGC is known to be mainly controlled by the five major tectonic zones. Four of them have almost similar ENE–WSW to E–W strike, but the fifth one has N–S strike coinciding with the trend of Rajmahal basin. From south to north they are named as the (i) South Purulia Shear Zone (SPSZ), (ii) North Purulia Shear Zone (NPSZ), (iii) Damodar graben and (iv) South Narmada South Fault (SNSF). Two schools of thought exist regarding the relationship between the Singhbhum craton and the CGC; one group favours CGC as a mobile belt[11–14] and the other favours the view that it is a cratonized mobile belt[15–20].

The area of present study is dominantly occupied by granites and gneisses along with enclaves of supracrustal rocks such as quartz mica schist, quartzite, quartz schist, calc silicate rocks, granulites and the tourmaline biotite schist. E–W trending meta-basic dykes are widespread and intrude the granites and gneisses. A few N–S trending unmetamorphosed gabbroic and lamprophyre dykes are also present intruding both meta-basic dykes and granite-gneisses. Some tourmaline-bearing quartz veins are also reported[21]. The presently studied N–S trending dyke is 1.5–2 m wide and about 200 m long, undeformed and unmetamorphosed gabbro dyke intrudes the Chhotanagpur-Granite-Gneisses in the Saghjohr village of Kersai Tehsil, Simdega district (Figure 1 *b*).

Alumina polished thin sections of the dyke rock were studied under a Carl Zeiss AXIO SCOPE.A1 polarizing microscope. CAMECA SX Five electron microprobe (EPMA) and EVO18 Scanning electron microscope (SEM) in the Department of Geology, Banaras Hindu University are used for imaging and mineral analyses. LIF, PET, LPET, LTAP and PC1 crystals of EPMA are used for quantification. Wavelength dispersive spectrometry and LaB6 filament with beam diameter of 1 µm were the analysing parameters. An accelerating voltage of 15 kV and a beam current of 10 nA (for both major and minor elements) were used. Standards like diopside (Ca), peridot (Mg), $SrSO_4$ (Sr), FeS_2 (Fe), orthoclase (K), rutile (Ti), NaCl (Na), apatite (P), $CaSiO_3$ (Si), corundum

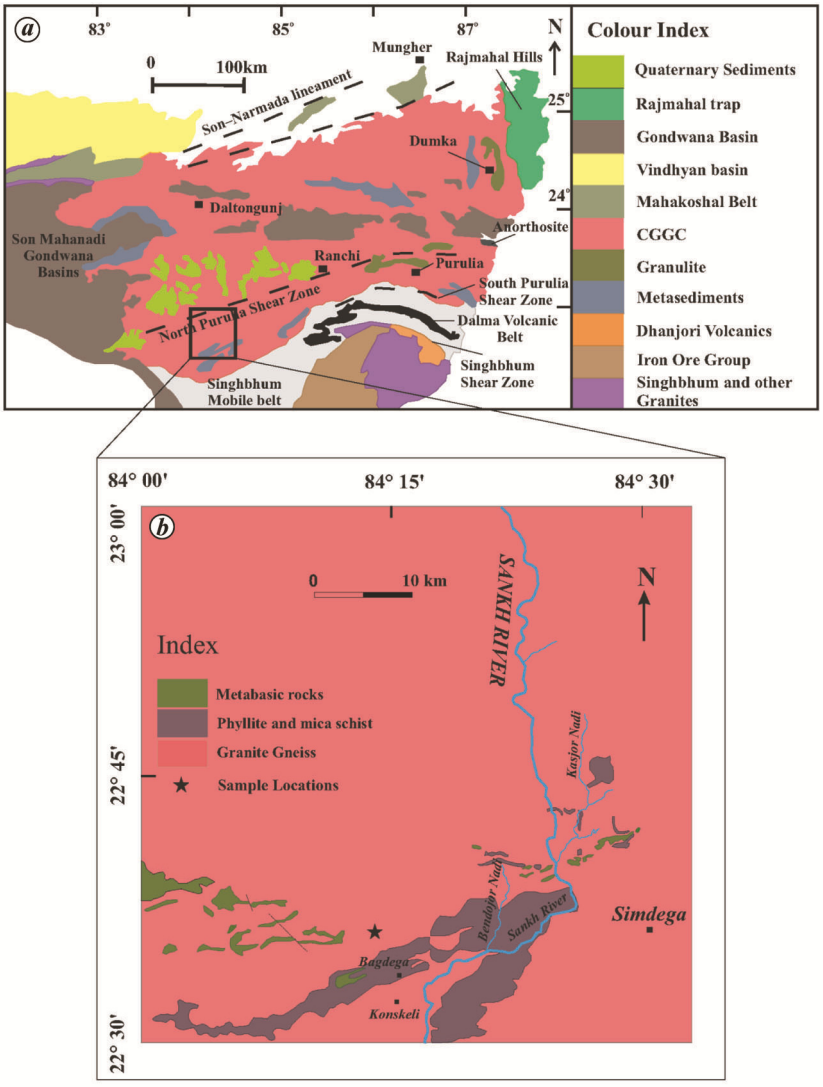

Figure 1. ***a***, A generalized geological map of Chotanagpur Gneissic Complex and nearby areas showing different litho-units[28]. ***b***, Geological map of the study area[29].

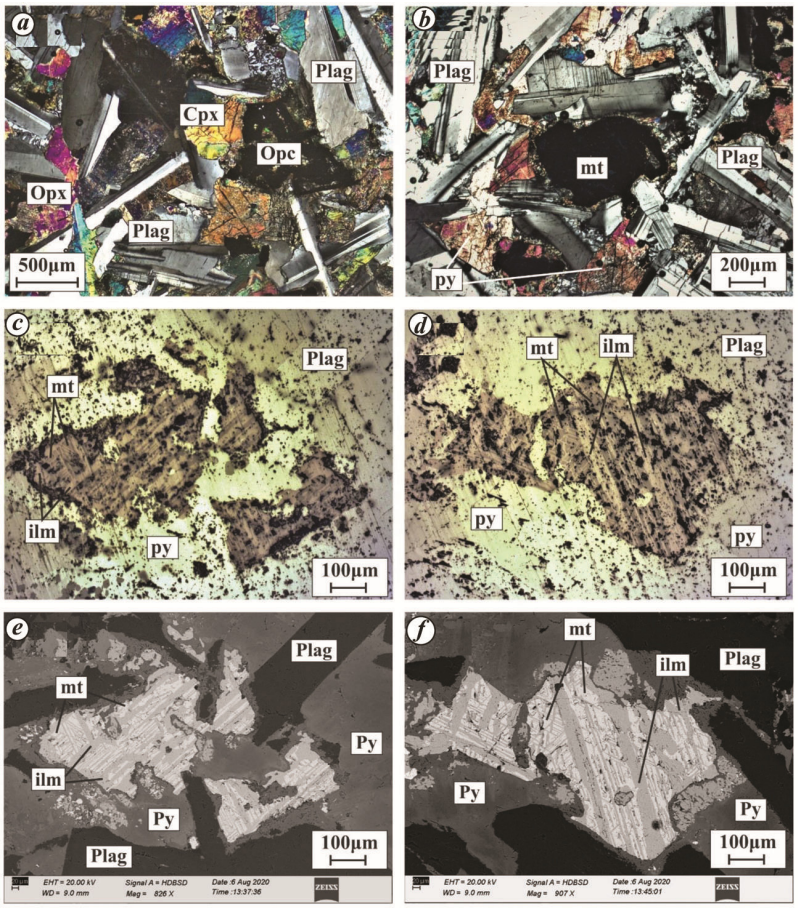

Figure 2. Petrographic photomicrographs and backscattered electron (BSE) images of Simdega gabbroic dyke. ***a***, ***b***, orthopyroxene (Opx) and clinopyroxene (Cpx) enclosed by the plagioclase in transmitted cross-polarized light. ***c***, ***d***, magnetite and ilmenite intergrowth texture in reflected light. ***e***, ***f***, BSE images of magnetite–ilmenite intergrowth pairs. Bright colour laminations are magnetite and relatively dark laminations are ilmenite. Plag, Plagioclase; Opc, Opaque; mt, magnetite; ilm, ilmenite.

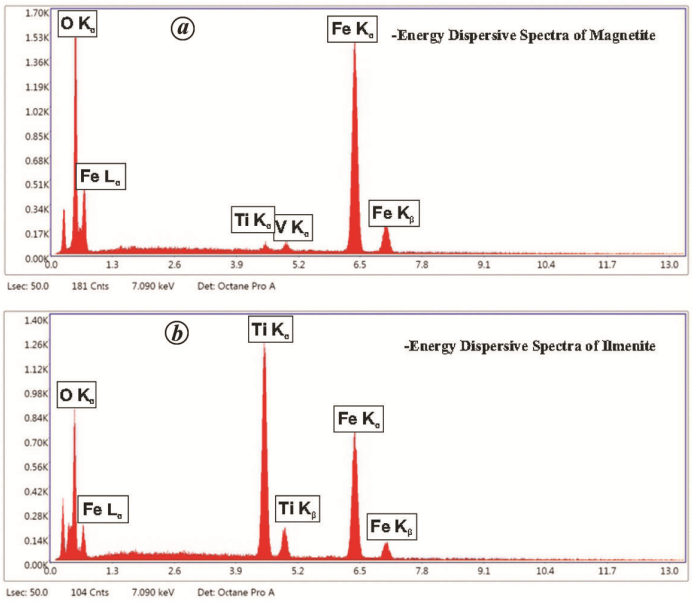

Figure 3. ***a***, Energy dispersive spectra (EDS) showing the presence of Fe, Ti, V. The Fe is very high relative to the Ti and V. ***b***, EDS spectra of ilmenite showing the high amount of Fe and Ti with the absence of V.

(Al), V_2O_3 (V) and fluorite (F) were used for calibration. Counting time was 10 sec for both major and minor elements. Vanadium is tested to prevent the interference with titanium in LIF and in LPET crystal. The error on the given calibration settings was expected to be <1% for major elements and <5% for trace elements.

Two gabbro samples were analysed for major and trace elements by ICPOES (Jarrell-Ash ENVIRO-II) and ICP-MS (Perkin Elmer Sciex ELAN 6000) at the Activation Laboratories, Ancaster, Canada. STM1, MRG1, DNC1, W2 and SY3 were the internal standards with the precision <5% and 5–10% for the major oxides and trace elements respectively.

Petrographic study shows that the gabbroic dyke of this study consists of clinopyroxene (25–30 vol%), orthopyroxene (4–5 vol%), plagioclase (35–40 vol%), minor amount of hornblende and opaque minerals. Magnetite and ilmenite essentially constitute the opaques. All the mineral phases are pristine and unaltered in nature. Coarse and tabular laths of plagioclase surround the pyroxenes. Lamellae of ilmenite in magnetite (Figure 2 *c*–*f*) are quite common.

Clinopyroxenes are subhedral, medium to coarse grained and are represented by augite, pigeonite and minor hedenbergite. Their composition varies from $Wo_{11.07}En_{23.21}Fs_{18.36}$ to $Wo_{37.15}En_{56.75}Fs_{53.08}$. Their TiO_2 content is high, i.e. 0.44–0.94 wt%. Orthopyroxene is ferrosilite and its composition ranges from $Wo_{1.07}En_{22.93}Fs_{63.41}$ to $Wo_{4.26}En_{35.40}Fs_{73.58}$. Plagioclase is dominantly andesine and labradorite with the compositional range from $An_{36.32}Ab_{62.58}Or_{1.10}$ to $An_{59.16}Ab_{40.26}Or_{0.58}$.

Lamellae of ilmenite in magnetite represent exsolution texture. Ilmenite has FeO 45.31–48.49 wt% and TiO_2 from 49.67 wt% to 51.77 wt%. On the other hand, magnetite displays a greater range of FeO varying from 31.59 wt% to 43.21 wt%, Fe_2O_3 from 40.28 wt% to 64.33 wt%; TiO_2 in magnetite is 0.96–13.18 wt% and contains unusually high V_2O_3 (1.85–4.47 wt%). In most grains V_2O_3 is in the range 1.5–2.5 wt%. While the vanadium-bearing titaniferous magnetite occurs as disseminated accessory phase in the dyke in the present study, such vanadiferous titano-magnetite ore bodies have also been reported from different domains of the Indian shield such as (i) Dublabera–Katwarpahar[2,3]

Table 1. Representative magnetite–ilmenite pairs mineral chemistry data from Simdega gabbroic dyke

Sample	SDG-52-1	SDG-52-1	SDG-52-1	SDG-52-1	SDG-52-1	SDG-52-1	SDG-52-1	SDG-52-1	SDG-52-1	SDG-52-1	SDG-52-2	SDG-52-2	SDG-52-1	SDG-52-1
Ponit#	104	105	112	111	115	116	122	121	123	124	188	189	315	316
	Magnetite	Ilmenite	Magnetite	Ilmenite	Magnetite	Ilmenite	Magnetite	Ilmenite	Magnetite	Ilmenite	Magnetite	Ilmenite	Magnetite	Ilmenite
SiO_2	0.06	0.02	0.08	0.01	0.06	0.04	0.10	0.01	0.05	0.00	0.10	1.12	0.00	0.00
TiO_2	1.09	51.51	0.96	50.85	1.29	51.58	1.32	51.29	1.52	51.77	1.38	49.67	3.89	51.56
Al_2O_3	0.37	0.01	0.59	0.00	0.25	0.00	0.37	0.00	0.33	0.00	0.64	1.27	0.35	0.01
$Fe_2O_3^*$	64.11	1.61	63.61	1.70	60.95	1.17	63.28	1.18	62.26	0.58	62.41	2.35	57.37	0.66
FeO*	32.09	45.73	31.99	45.16	32.24	46.04	32.48	45.54	32.22	46.14	32.23	44.73	34.37	45.66
MnO	0.00	0.46	0.00	0.39	0.00	0.27	0.00	0.45	0.00	0.33	0.04	0.65	0.04	0.60
V_2O_3	1.85	0.00	2.09	0.00	4.47	0.00	2.21	0.00	2.22	0.00	2.17	0.00	2.81	0.64
Sum	99.58	99.34	99.32	98.11	99.25	99.11	99.76	98.47	98.60	98.82	98.98	99.80	98.84	99.12
O_2 anions	4	3												
Si	0.00	0.00	0.00	0.00	0.00	0.00	0.00	0.00	0.00	0.00	0.00	0.03	0.00	0.00
Ti	0.03	0.98	0.03	0.98	0.04	0.99	0.04	0.99	0.04	0.99	0.04	0.93	0.11	0.99
Al	0.02	0.00	0.03	0.00	0.01	0.00	0.02	0.00	0.01	0.00	0.03	0.04	0.02	0.00
Fe^{+3}	1.86	0.03	1.84	0.03	1.77	0.02	1.83	0.02	1.82	0.01	1.81	0.04	1.66	0.01
Fe^{+2}	1.03	0.97	1.03	0.97	1.04	0.98	1.04	0.98	1.05	0.99	1.04	0.93	1.11	0.97
Mn	0.00	0.01	0.00	0.01	0.00	0.01	0.00	0.01	0.00	0.01	0.00	0.01	0.00	0.01
V	0.06	0.00	0.06	0.00	0.14	0.00	0.07	0.00	0.07	0.00	0.07	0.00	0.09	0.01
Total	3.00	2.00	3.00	2.00	3.00	2.00	3.00	2.00	3.00	2.00	3.00	2.00	3.00	2.00
Mol % Usp	0.03		0.03		0.04		0.04		0.05		0.04		0.11	
Mol % Ilm	0.98		0.98		0.99		0.99		0.99		0.96		0.99	
After Spencer and Lindsley[24]														
Temp (°C)	482		479		462		459		412		564		486	
$\log_{10} fO_2$	–27		–27		–29		–30		–35		–21		–28	

(V_2O_5 = 0.59–4.9 wt%), Kumardhubi (V_2O_5 = 1.4 wt%), Betjharan (V_2O_5 = 1.0 wt%), Amdabera[4,5] (V_2O_5 = 0.7–1.5 wt%), Nausahi[7,8] (V_2O_5 = 0.96–1.88 wt%) and Saltora[6] areas of the Singhbhum craton, (ii) from the Nuggihali schist belt (V_2O_5 = 0.45–1.0 wt%), Dharwar craton, southern India[9,10] and (iii) Ganjang, Karbi–Anglong (V_2O_5 = 0.07–2.14 wt%) from the Meghalaya plateau[22].

The reported gabbroic dyke is classified as gabbro-norite based on mineralogy and whole rock data. The bulk rock composition (major oxides) of the dyke is: SiO_2 = 50.52 wt%, Al_2O_3 = 12.77 wt%, $Fe_2O_3^T$ = 17.02 wt%, MgO = 5.4 wt%, CaO = 10.05 wt%, TiO_2 = 2.27 wt%, Na_2O = 2.3 wt%, K_2O = 0.63 wt%. The bulk rock data shows high abundance of V = 398 ppm.

Pristine and unaltered mineralogy in all the studied samples demonstrate lack of role of hydrothermal fluid activity. During crystallization of the melt in the magma chamber, V can enter either the Fe^{3+} site in Fe_3O_4 or the Al^{3+} position in the spinel structure. V also can enter the Ti^{4+} position in $FeTiO_2$ subject to fO_2 conditions in the magma chamber[23]. Energy dispersive spectra (EDS) of magnetite and ilmenite clearly reveal the preference of V towards the Fe^{3+} (Figure 3). The substitution was nearly consistent at constant fO_2 conditions as also revealed by limited variation in concentration. This is further supported by the poor correlation between the element oxides such as Al_2O_3 and TiO_2 vs V_2O_3 (not shown).

The calculation of equilibrium temperature and oxygen fugacity using ilmenite–magnetite pairs is carried out following Spencer and Lindsley[24] wherein iron, ulvospinel and ilmenite have been recalculated after Carmichael[25]. The results are shown in Table 1. V is dominantly present as V^{3+} in oxygen fugacity conditions below the hematite–magnetite (HM) buffer. Hence, V^{3+} is likely to be incorporated within magnetite, rather than in ilmenite. Preferential enrichment of vanadium in magnetite would have occurred during exsolution at late-stage of magmatic crystallization/cooling in the temperature range of 412–564°C and under relatively lower oxygen fugacity (log fO_2 = –35 to –21) condition (Figures 4 and 5). Whereas favourable oxygen fugacity conditions may have prevailed for the formation of vanadium-bearing titaniferous magnetite in this dyke, economically viable concentration of this mineral additionally requires other conditions such as large enough magmatic body and tectono-magmatic conditions which promote concentration of the ore minerals into ore bodies. Detailed regional geological and geophysical studies in this region are required to ascertain the presence of such ore bodies which are known to be economically prospective[26,27].

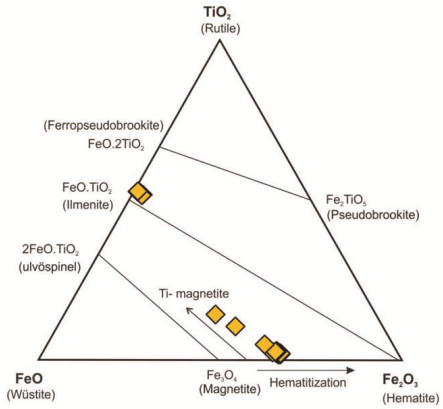

Figure 4. Composition of Fe–Ti oxides plotted in TiO_2–FeO–Fe_2O_3 ternary diagram (atomic proportions)[30].

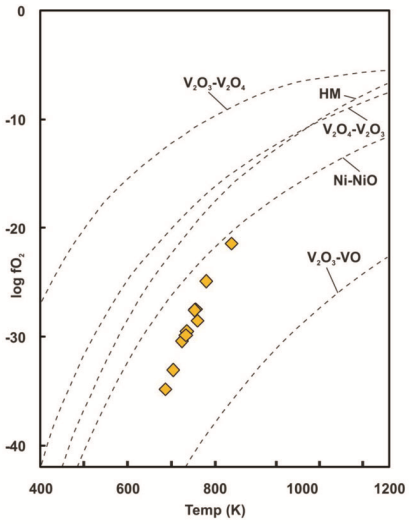

Figure 5. T-fO_2 diagram[31] showing the study samples are in the ideal condition of formation of magnetite–ilmenite pairs.

1. Chakraborty, K. L., Roy, J. and Majumder, T., *J. Geol. Soc. India*, 1988, **31**, 305–313.
2. Dunn, A. J. and Dey, A. K., *Trans. Min. Geol. Soc. India*, 1937, **31**, 130–161.
3. Dasgupta, H. C., *J. Geol. Min. Met. Soc. India*, 1969, **41**(2), 51–64.
4. Roy, S., *Proc. Nat. Inst. Sci*., 1959, **20**(6), 691–702.
5. Banerjee, P. K., *Chem. Geol*., 1984, **43**, 257–269.
6. Bose, M. K. and Roy, A. K., *Econ. Geol*., 1966, **61**, 555–562.
7. Mukherjee, S., *J. Geol. Min. Met. Soc. India*, 1958, **30**, 109–124.
8. Chakraborty, K. L., *Proc. Nat. Inst. Sci. India*, 1959, **25**/**A**, 262–272.
9. Chakraborty, K. L., *Indian Mineral.*, 1961, **2**, 28–35.
10. Vasudev, V. N. and Srinivasan, R., *J. Geol. Soc. India*, 1979, **20**, 170–178.
11. Mahadevan, T. M., *Geology of Bihar and Jharkhand*, Geological Society of India (Text book series), 2002, p. 564.
12. Ghose, N. C. and Chatterjee, N., *Indian Dykes: Geochemistry, Geophysics and Geochronology* (eds Srivastava, R. K., Sivaji, Ch. and Chalapathi Rao, N. V.), Narosa Publishers, New Delhi, 2008, pp. 471–493.

13. Ghose, N. C., In *Recent Researches in Geology* (ed. Sinha-Roy, S.), Hindustan Publishing Corporation, Delhi, 1983, vol. 10, pp. 211–247.
14. Mukhopadhyay, D., *Precambrian of the Eastern Indian Shield*, Geological Society of India Memoir, 1988, **8**, 237.
15. Naqvi, S. M. and Rogers, J. J. W., *Precambrian Geology of India*, Oxford Univ. Press, 1987, p. 223.
16. Kumar, A. and Ahmad, T., *Geochem. J.*, 2007, **41**, 173–186.
17. Sharma, R. S., *Cratons and Fold Belts of India*, Springer-Verlag, 2009, p. 304.
18. Srivastava, R. K., Kumar, S. and Sinha, A. K., *J. Earth Syst. Sci.*, 2012, **121**, 509–523.
19. Srivastava, R. K., Kumar, S., Sinha, A. K. and Chalapathi Rao, N. V., *J. Asian Earth Sci*., 2013, **84**, 34–50.
20. Chalapathi Rao, N. V., Srivastava, R. K., Sinha, A. K. and Ravikant, V., *Earth Sci. Rev*., 2014, **136**, 96–120.
21. Kumar, D., Pandit, D., Sharma, A. and Chalapathi Rao, N. V., *Curr. Sci.*, 2019, **117**(5), 858–865.
22. Saha, A., Ganguly, S., Ray, J. S. and Dhang, A., *J. Geol. Soc. India*, 2010, **76**, 26–32.
23. Banerjee, P. K., *Chem. Geol*., 1984, **43**, 257–269.
24. Spencer, K. J. and Lindsley, D. H., *Am. Mineral.*, 1981, **66**(11–12), 1189–1201.
25. Carmichael, I. S. E., *Contrib. Mineral. Petrol*., 1967, **14**(1), 36–64.
26. Mohanty, J. K., Khaoash, S., Singh, S. K., Sahoo, P. K. and Paul, A. K., *India Scan. J. Metal.*, 1999, **28**(6), 254–259.
27. Devaraju, T. C., Viljoen, R. P., Sawkar, R. H. and Sudhakara, T. L., *J. Geol. Soc. India*, 2009, **73**, 73–100.
28. Acharyya, S. K., *Gondwana Res.*, 2003, **6**(2), 197–214.
29. Ray, J. N., Geological Survey of India map of Raurkela Quadrangle – Bihar, Madhya Pradesh and Orissa. Toposheet number 73B, 1983.
30. Ondrejka, M., Broska, I. and Uher, P., *Acta Geol. Slovaca*, 2015, **7**(1), 51–61.
31. Schuiling, R. D. and Feenstra, A., *Chem. Geol.*, 1980, **30**, 143–150.

ACKNOWLEDGEMENTS. We thank the Head, Department of Geology, BHU, Varanasi for the departmental support. N.V.C.R. thanks DST-SERB for granting research project (IR/S4/ESF-18/2011 dated 12.11.2013). D.K. thanks CSIR, New Delhi for the award of JRF (NET) and SRF. We also thank Dr Ajit K. Sahoo (BHU) for useful discussions. Constructive review by an anonymous journal reviewer is thankfully acknowledged.

Received 1 December 2020; revised accepted 12 January 2021

DEEPAK KUMAR
DINESH PANDIT
N. V. CHALAPATHI RAO*

Department of Geology,
Institute of Science,
Banaras Hindu University,
Varanasi 221 005, India
**For correspondence.*
e-mail: nvcrao@bhu.ac.in

Molecular phylogeny of *Scymnus latifolius*, a predator species of mealy bug shows divergent evolution among *Scymnus* species

Ladybird beetles belong to the family Coccinellidae, super family Cucujoidea, suborder Polyphaga of order Coleoptera[1], and consist of more than 360 genera and 6000 species[2]. Many of the coccinellid insects are widely used as predators in the biological control of major agricultural pests. Previously, we have described a novel predator, *Scymnus* (*Pullus*) *latifolius* Poorani belonging to Scymnini tribe of the family Coccinellidae[3]. The *S. latifolius* beetle is found to predate upon all developmental stages of several mealybug species, a major pest with a wide host range, and hence could play a key role in biological control.

Several phylogenetic subdivisions for the family Coccinellidae have been proposed based on conventional morphological observations[2,3] and molecular methods[4,5]. Mitochondrial gene sequences have been widely used to understand the evolutionary history of coleopterans[6,7] and coccinellids in particular[4,5,8,9]. The mitochondrial cytochrome *C* oxidase subunit I (COI) gene nucleotide sequences have been extensively used for phylogenetic analysis and species-level identification of Coccinellidae[9]. The present study was conducted to identify the phylogenetic relationship of *Scymnus* species with other Scymnini and coccinellids through comparative analysis of partial sequences of mitochondrial COI gene.

Insect collections were obtained from mulberry gardens located in Murshidabad, Malda, Birbhum and Nadia districts, West Bengal, India using standard techniques. Adult specimens of *S. latifolius* were positively identified using morphological descriptions[2] and preserved in 85% ethanol in the dark at 4°C until further analysis. DNA was isolated from the hind legs of individual beetles using a DNA isolation kit (Qiagen, Germany) following the manufacturer's protocol and stored at –20°C until use. Polymerase chain reaction (PCR) amplification of partial gene sequences of mitochondrial COI gene was conducted using the universal COI primers[10] following a method described previously[11]. The PCR products were purified using a kit (Qiagen, Germany) and sequenced by Sanger's method at a commercial facility. The nucleotide sequences of COI gene generated have been submitted to the National Center for Biotechnology Information (NCBI) and can be accessed at GenBank (accession number KU512906). Sequence diversity of specific 595 bp fragment of the mitochondrial COI gene (the COI 5′ region) amplified from *S. latifolius* was compared with COI gene sequences of 44 different Coccinellids with one out-group from another subfamily (*Serangium* spp.) available in the NCBI database. The initial multiple alignment and sequence editing were carried out using Molecular Evolutionary Genetics Analysis software (MEGAX)[12]. Later, phylogenetic analysis was carried out employing Bayesian approaches[13] using Mr Bayes programme (Mr Bayes 3.2.7v WIN64) available at https://nbisweden.github.io/MrBayes/download.html. Before constructing the phylogenetic tree, the substitution model was analysed using MEGAX software. The model GTR + I + G was found to fit well with lowest Bayesian inference (BI) index. BI analyses were done using two runs simultaneously, with maximum likelihood starting tree, and four chains were used for the analysis (one cold and three hot) and the temperature set at 0.1. A run was